



The mapping and differentiation of biological and environmental elemental signatures in the fossil remains of a 50 million year old bird

Journal:	<i>Journal of Analytical Atomic Spectrometry</i>
Manuscript ID:	JA-ART-10-2014-000395.R1
Article Type:	Paper
Date Submitted by the Author:	15-Jan-2015
Complete List of Authors:	<p>Egerton, Victoria; University of Manchester, School of Earth, Atmospheric and Environmental Science Wogelius, Roy; University of Manchester, School of Earth, Atmospheric and Environmental Science Norell, Mark; American Museum of Natural History, Division of Paleontology Edwards, Nicholas; University of Manchester, School of Earth, Atmospheric and Environmental Science Sellers, William; University of Manchester, Faculty of Life Sciences Bergmann, Uwe; SLAC National Accelerator Laboratory, Sokaras, Dimosthenis; SLAC National Accelerator Laboratory, Stanford Synchrotron Radiation Lightsource Mori, Roberto; Stanford Synchrotron Radiation Lightsource, SLAC National Accelerator Laboratory, Ignatyev, Konstantin; Diamond Light Source, van Veelen, Arjen; University of Manchester, School of Earth, Atmospheric and Environmental Science Anne, Jennifer; University of Manchester, School of Earth, Atmospheric and Environmental Science van Dongen, Bart; University of Manchester, School of Earth, Atmospheric and Environmental Science Knoll, Fabien; University of Manchester, School of Earth, Atmospheric and Environmental Science Manning, Phillip; University of Manchester, School of Earth, Atmospheric and Environmental Science</p>

	High Z Elements								Low Z Elements				
	Element weight %		ppmW						Element weight %				
	Ca	Fe	Mn	Ni	Cu	Zn	As	Pb	Si	P	S	Cl	
Matrix	23.1	0.23	40	11	6	44	22	63	2.75	0.09	0.08	0.03	Matrix
Bone (2)	37.9	0.11	211	13	6	51	18	53	1.28	9.25	0.44	0.01	Bone (9)
Feather (1)	19.5	0.37	918	59	47	63	28	64	2.56	0.15	1.4	0.1	Feather (10)
Feather (3)	21.1	0.25	130	12	36	64	26	85	2.52	0.13	1.05	0.07	Feather (11)
Feather (5)	24.6	0.38	963	62	140	95	22	65	3.11	0.09	0.71	0.1	Feather (12)
Feather (6)	18.7	0.52	522	107	394	87	29	83					
Orbit	14.6	0.08	193	88	225	93	21	58					

1
2
3
4
5
6
7
8
9
10
11
12
13
14
15
16
17
18
19
20
21
22
23
24
25
26
27
28
29
30
31
32
33
34
35
36
37
38
39
40
41
42
43
44
45
46
47
48
49

	High Z Elements								Low Z Elements				
	Element weight %		ppmW						Element weight %				
	Ca	Fe	Mn	Ni	Cu	Zn	As	Pb	Si	P	S	Cl	
Matrix	23.1	0.23	40	11	6	44	22	63	2.75	0.09	0.08	0.03	Matrix
Bone (2)	37.9	0.11	211	13	6	51	18	53	1.28	9.25	0.44	0.01	Bone (9)
Feather (1)	19.5	0.37	918	59	47	63	28	64	2.56	0.15	1.4	0.1	Feather (10)
Feather (3)	21.1	0.25	130	12	36	64	26	85	2.52	0.13	1.05	0.07	Feather (11)
Feather (5)	24.6	0.38	963	62	140	95	22	65	3.11	0.09	0.71	0.1	Feather (12)
Feather (6)	18.7	0.52	522	107	394	87	29	83					
Orbit	14.6	0.08	193	88	225	93	21	58					

Table 1: XRF Point Analyses. The numbers beside the feature correspond to the points marked on Figure 1a. Beamline geometry is calibrated using a Durango apatite standard. 2σ errors, calculated from counting statistics, are approximately 8% relative for the light elements (Ca, Si, P, S, Cl) and 5% for all of the trace metals except Pb. (For example, the Ca wt. % in the bone is $37.9 \pm 3\%$ while the Zn concentration is 51 ± 2.6 ppm.) Errors on Pb, due to overlap with As and rising background caused by the elastic and Compton scattering peaks, are much larger at approximately 25% (using the bone example: 64 ± 16 ppm).

57x18mm (300 x 300 DPI)

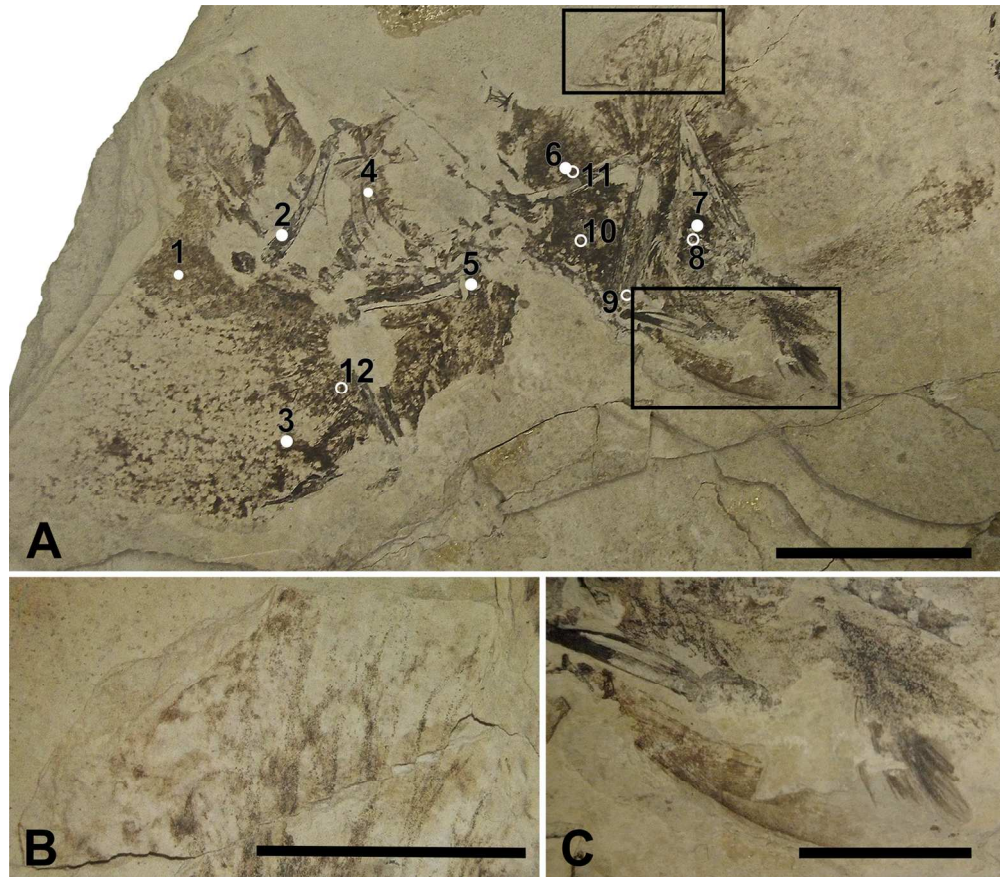


Figure 1: AMNH FARB 30806. (A) Coliiformes bird (AMNH FARB 30806) from the Green River Formation, Fossil Butte Member. The numbers correspond to where point data was taken for High Z (1-7) and Low Z (8-12) elements. Scale bar = 5 cm. (B) Magnified view of the upper box containing the feather sample obtained for SEM. (C) Magnified view of well preserved feathers. (B-C) Scale bar = 2 cm.
149x130mm (300 x 300 DPI)

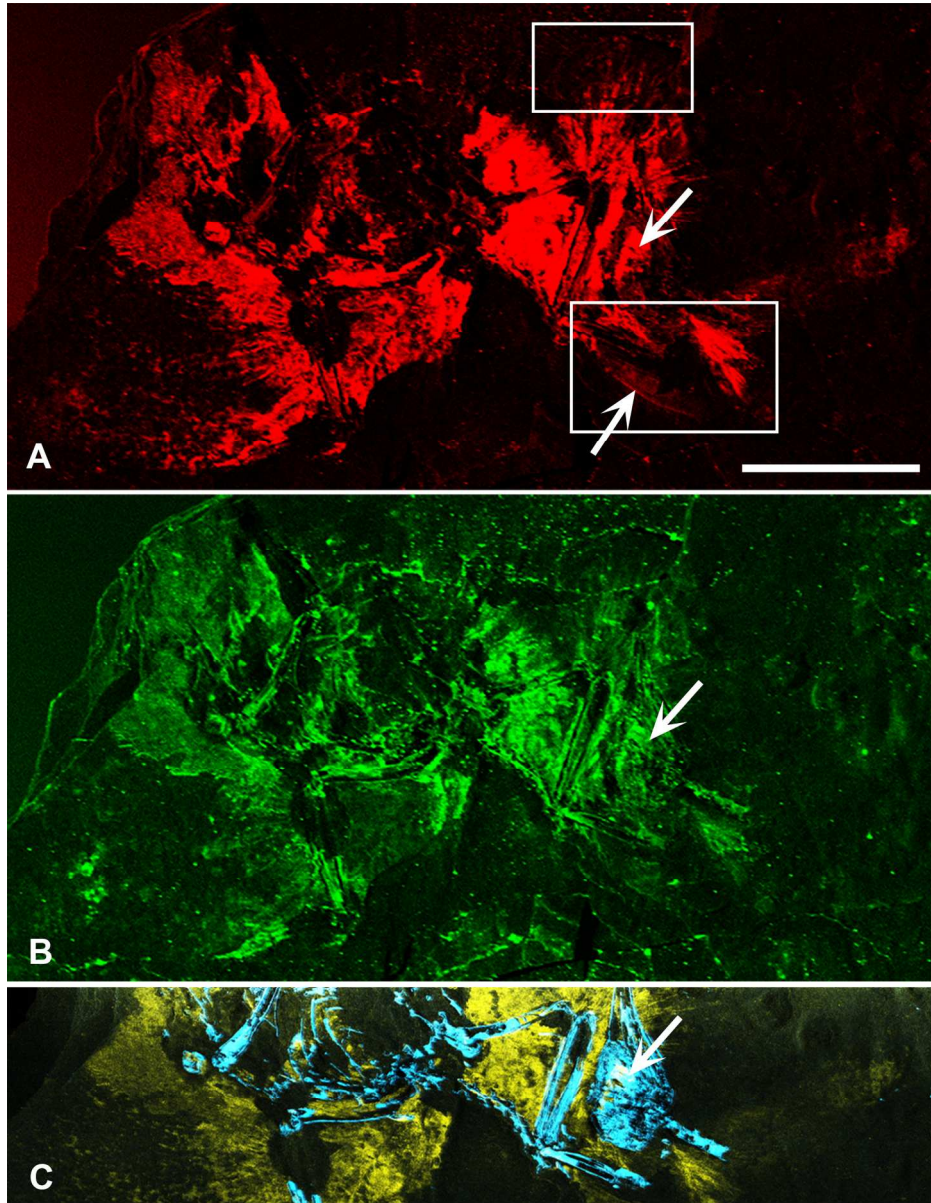


Figure 2: SRS-XRF Elemental maps of AMNH FARB 30806. (A) Copper (red) and (B) zinc (green) maps showing the relative intensities of the elements mapping distinctly within the feathers. (A) The upper box in copper corresponds to Figure 1b, while the lower box corresponds to Figure 1c. The lower arrow is pointing to the rachis of a feather. (C) Phosphorus (blue) and sulfur (yellow) elemental map distinctly showing bone with higher intensities of phosphorus and the feathers containing higher intensities of sulfur. (A-C) Upper arrow is pointing to the orbit (eye socket). Scale bar = 5 cm.
219x283mm (300 x 300 DPI)

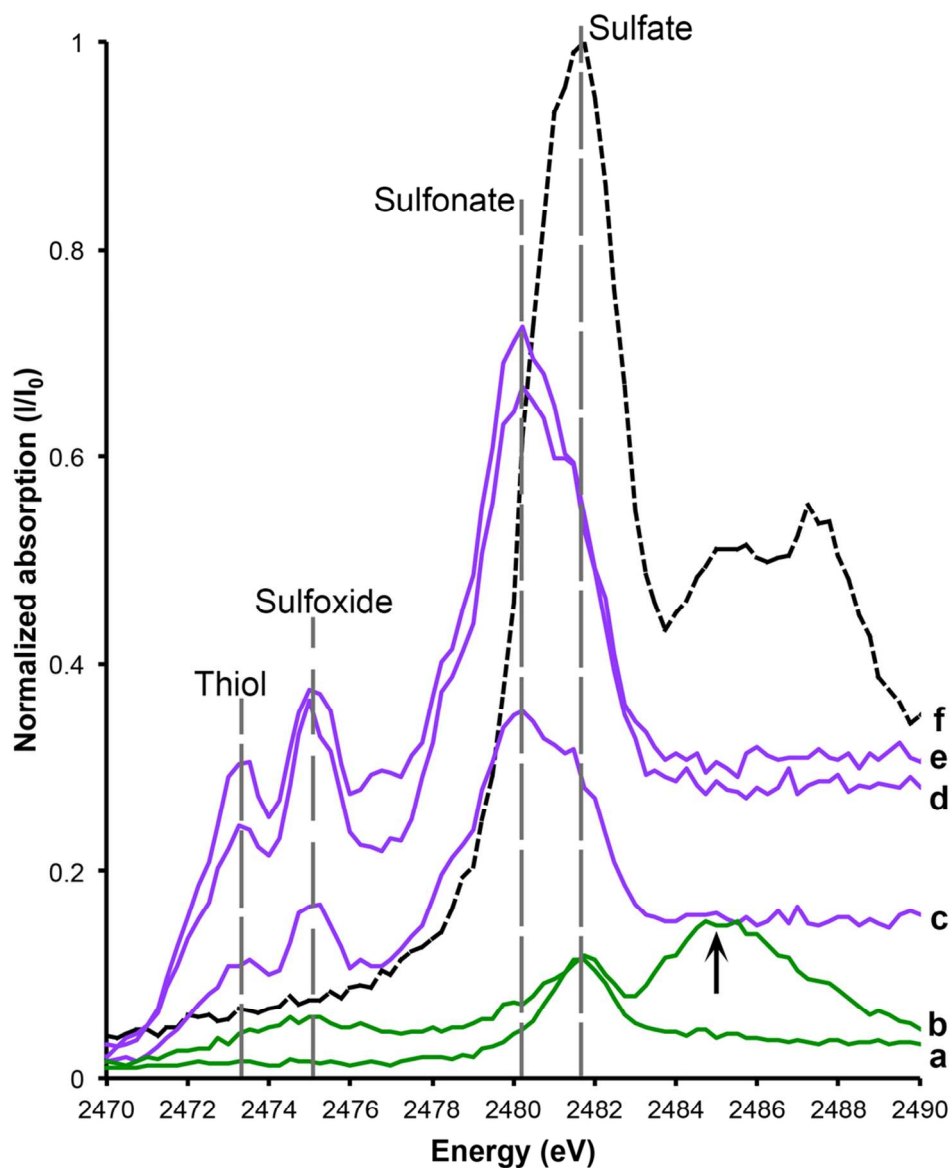


Figure 3: Sulfur XANES for AMNH FARB 30806. The relative abundance of sulfur within the matrix (a-b) and feathers (c-e) has been calibrated to a sulfur standard, K_2SO_4 (f). The data are normalized to raw intensity I/I_0 . The two matrix samples both have peaks that correspond with the sulfate standard, while the feathers contain abundant sulfonate, sulfoxide and thiol relative to the matrix samples. The lower matrix spectrum (a) shows an elongate organic peak across both sulfoxide and thiol due to the breakdown of organics. The upper matrix spectrum (b) has an additional peak at 2485 eV, which is due to Pb substitution for Ca in $CaSO_4$.

99x118mm (300 x 300 DPI)

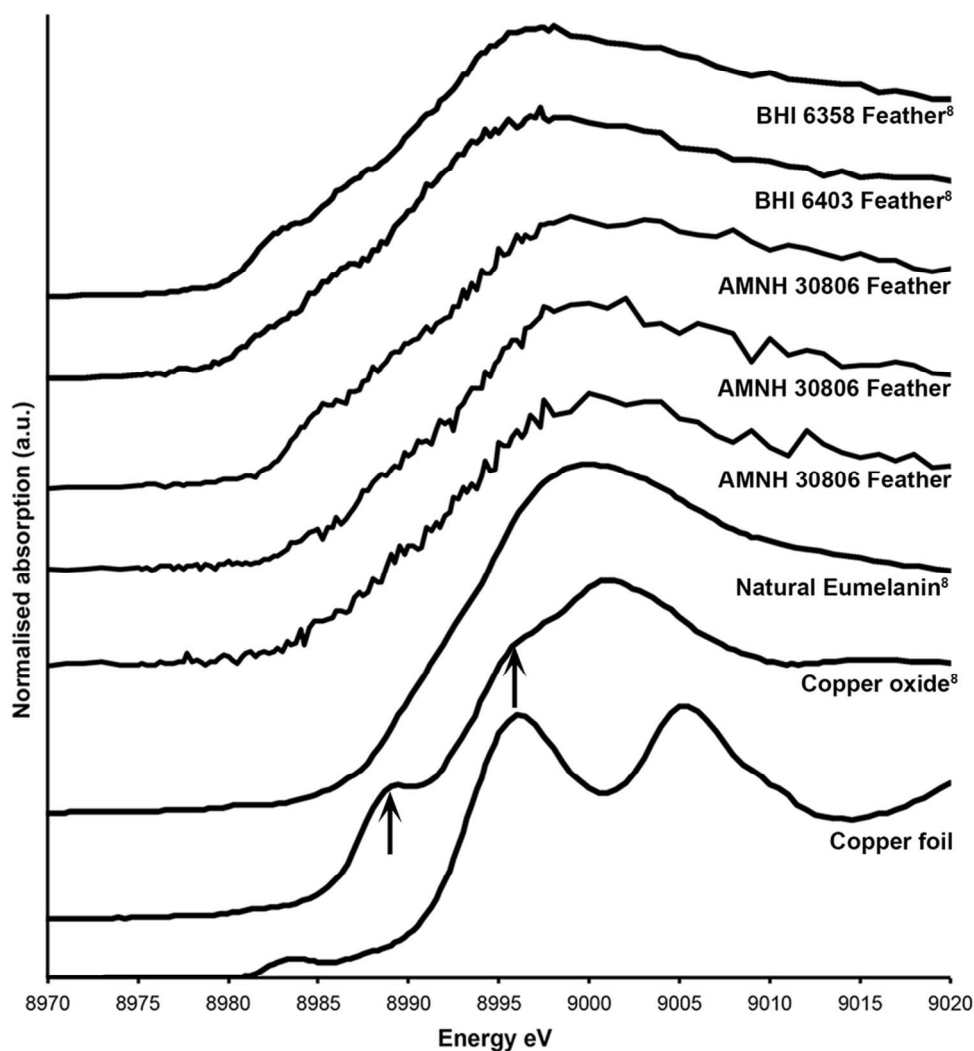


Figure 4: Copper XANES spectra. Cu XANES spectra are from a copper standard (copper foil) and three different feathers from AMNH FARB 30806. The spectra from these have been plotted along with published spectra from copper oxide, natural copper eumelanin, and two isolated feathers from the Green River Formation (BHI 6358 and 6403)⁸. The arrows on the copper oxide are pointing to peaks that are unique to that spectrum and do not occur in the fossil material.

91x100mm (300 x 300 DPI)

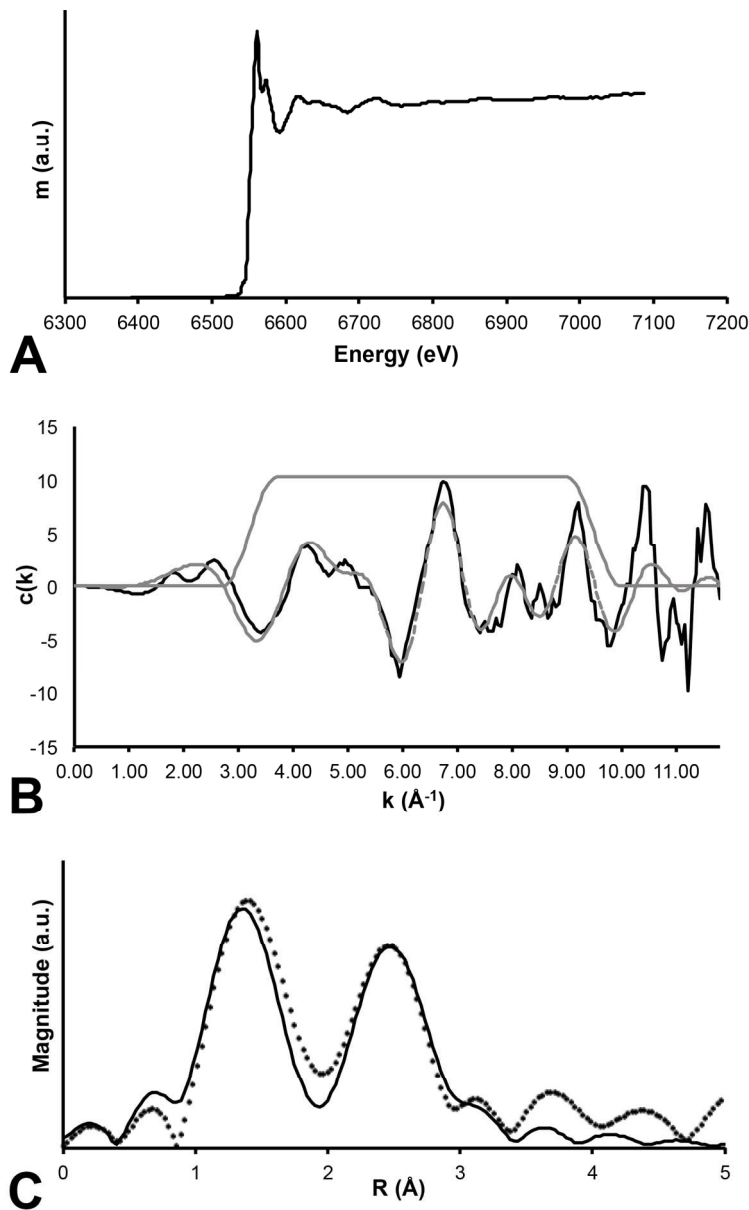


Figure 5: Mn EXAFS. Three panel results of EXAFS analysis of Mn within the fossil specimen. (A) Raw data for the absorption coefficient measurement at the Mn K-edge. (B) EXAFS function presented for the specimen (solid line) and a computed fit to the data (dashed line). (C) Fourier transform of EXAFS where the data are presented as the discrete points and the best fit is shown as the thin solid line. Clearly the RDF shows two strong backscattering shell surrounding the central Mn absorber.
131x208mm (300 x 300 DPI)

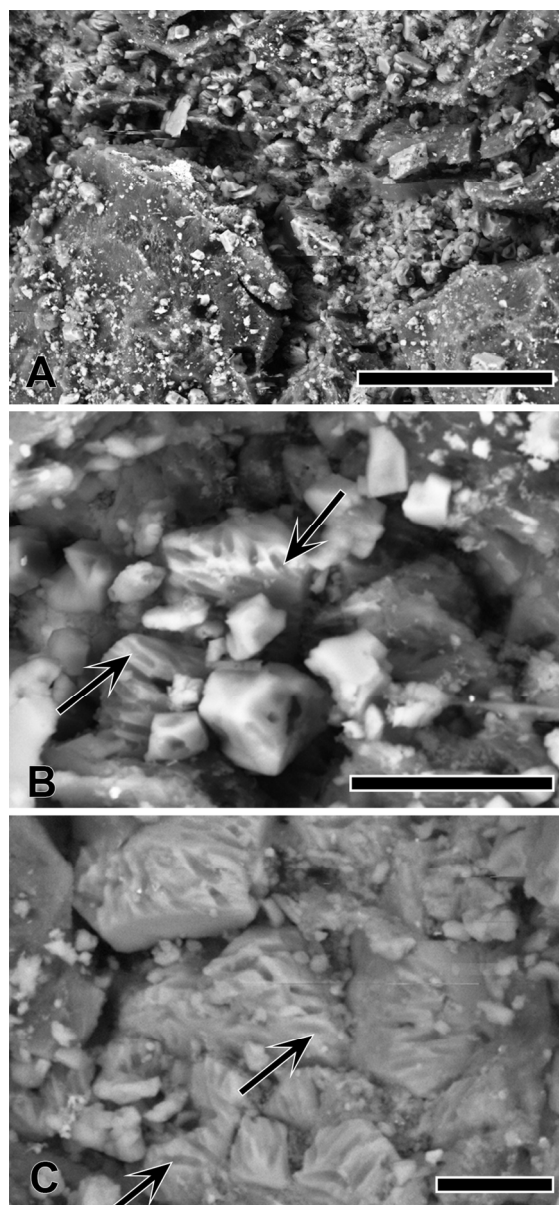


Figure 6: SEM of feathers from AMNH FARB 30806. (A) Secondary electron image of a carbonaceous film, mineral crystals and possible eumelanosomes (arrow). Scale bar = 50 μm . (B) Backscattered electron image of possible eumelanosome preservation (arrow). Scale bar = 10 μm . (C) Secondary electron image of possible eumelanosome preservation (arrow). Scale bar = 5 μm .
178x383mm (300 x 300 DPI)

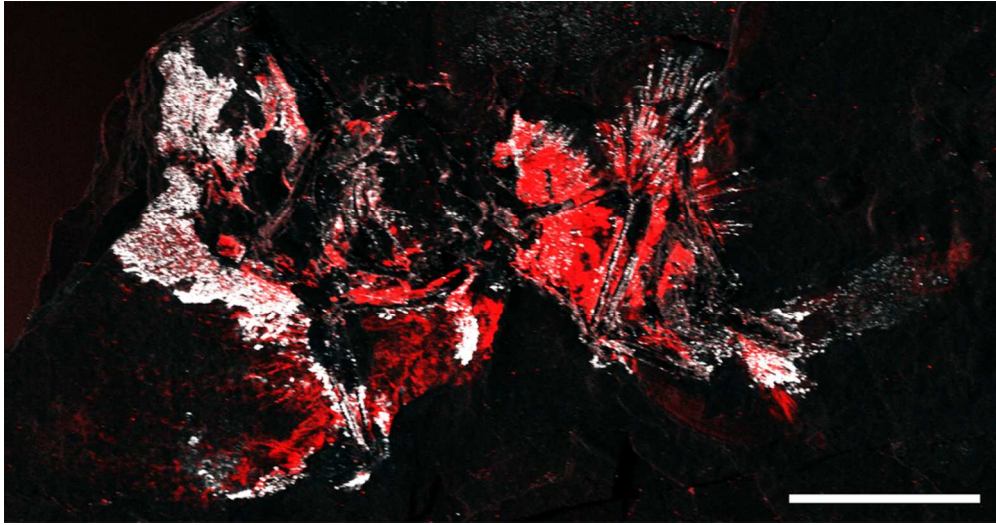


Figure 7: Copper and manganese elemental map of AMNH FARB 30806. Copper (red) and manganese (white) both appear to map within the feathers; however correlation between the two show no significance in the distribution. Scale bar = 5 cm.
88x46mm (300 x 300 DPI)

1
2
3
4
5
6
7
8
9
10
11
12
13
14
15
16
17
18
19
20
21
22
23
24
25
26
27
28
29
30
31
32
33
34
35
36
37
38
39
40
41
42
43
44
45
46
47
48
49
50
51
52
53
54
55
56
57
58
59
60

1 **The mapping and differentiation of biological and environmental elemental signatures in**
2 **the fossil remains of a 50 million year old bird**

3
4
5 Victoria M. Egerton^{1*}, Roy A. Wogelius¹, Mark A. Norell², Nicholas P. Edwards¹, William I.
6 Sellers³, Uwe Bergmann⁴, Dimosthenis Sokaras⁵, Roberto Alonso-Mori⁴, Konstantin Ignatyev⁶,
7 Arjen van Veelen¹, Jennifer Anné¹, Bart van Dongen¹, Fabien Knoll¹ and Phillip, L. Manning^{1,2}

8
9 ¹University of Manchester, School of Earth, Atmospheric and Environmental Sciences,
10 Williamson Research Centre for Molecular Environmental Science, Manchester M13 9PL, UK

11 ²American Museum of Natural History, Division of Paleontology, New York 10024-5192, USA

12 ³University of Manchester, Faculty of Life Sciences, Manchester M13 9PL, UK

13 ⁴SLAC National Accelerator Laboratory, Linac Coherent Light Source, Menlo Park, CA, 94025,
14 USA

15 ⁵SLAC National Accelerator Laboratory, Stanford Synchrotron Radiation Lightsource, Menlo
16 Park, CA 94025, USA

17 ⁶Diamond Light Source, Didcot, OX11 0DE, UK

18
19 *Corresponding author victoria.egerton@manchester.ac.uk

20
21 **1. ABSTRACT**

22 The preservation of fossils reflects the interplay of inorganic and organic chemical processes,
23 which should be clearly differentiated to make interpretations about the biology of extinct
24 organisms. A new coliform bird (mouse bird) from the ~50 million year old Green River
25 Formation (Wyoming, USA) has here been analysed using synchrotron x-ray fluorescence and
26 environmental scanning electron microscopy with an attached x-ray energy dispersive system
27 (ESEM-EDS). The concentration and distribution of 16 elements (Si, P, S, Cl, K, Ca, Ti, Mg, Fe,
28 Ni, Cu, Zn, As, Br, Ba, Hg) has been mapped for individual points on the sample. S, Cu and Zn
29 map distinctly within visibly preserved feathers and X-ray Absorption Spectroscopy (XAS)
30 shows that S and Cu within the feathers are organically bound in a similar manner to modern
31 feathers. The morphological preservation of the feathers, on both macro- and microscopic scales,

1
2
3 1 is variable throughout the fossil and the differences in the lateral microfacies have resulted in a
4 2 morphological preservation gradient. This study clearly differentiates endogenous organic
5 3 remains from those representing exogenous overprinted geochemical precipitates and illustrates
6 4 the chemical complexity of the overall taphonomic process.
7
8
9
10
11
12
13

14 7 **2. INTRODUCTION**

15 8
16
17

18 9 Fossils are formed through a complex system of physical and chemical changes that
19 10 begin at the moment of an organism's death. Taphonomy (literally 'burial-laws') is the study of
20 11 such changes and interactions on the buried remains of an organism. The taphonomic changes
21 12 are controlled by the environment in which the organism is buried and by the biological tissues
22 13 constructing the organism. Mineralized or 'hard' tissue, like bone, shell, and teeth, are more
23 14 easily preserved due a combination of their crystalline structure and chemistry¹. However, soft
24 15 tissue preservation is rare and restricted to a narrow selection of environmental regimes. In
25 16 terrestrial environments, exceptional preservation can occur in lacustrine (lake) environments
26 17 due to the low energy and reduced-oxygen conditions in such depositional systems^{1,2}. Reduced
27 18 oxygen helps to inhibit bacterial activity and tissue decay while favouring mineral precipitation
28 19 around the tissues of the organism^{1,3}.
29
30
31
32
33
34
35
36

37 20 The Green River Formation consists of limestone deposits extending over 65,000 square
38 21 kilometers across Utah, Colorado, Wyoming and Idaho⁴. The Formation consists of a series of
39 22 three Eocene lakes: Uinta, Gosiute and Fossil Lakes. Super-saturation of calcium carbonate
40 23 within the lakes from rivers flowing from the proto-Rocky Mountains caused the deposition of
41 24 this carbonate succession. A diverse community of mammals, birds, reptiles, amphibians and
42 25 fishes that lived in and around the have been preserved in this carbonate succession. Local
43 26 reduced oxygen conditions within the lakes facilitated the preservation of these organisms⁴. Here
44 27 we discuss the excellent preservation of an Eocene Coliiformes bird and examine the complexity
45 28 of its preservation from a standpoint of both the endogenous biochemistry and exogenous
46 29 geochemistry.
47
48
49
50
51
52
53
54
55
56
57
58
59
60

31 3. METHODS

3.1. Sample

The fossilized remains of a mousebird (Coliiformes) (Figure 1) were examined from the collections of the American Museum of Natural History, New York, USA (AMNH FARB 30806). This specimen was collected from the ~50 million year old Fossil Butte Member (Fossil Lake) of the Green River Formation, on the Lewis Ranch, Lincoln County, Wyoming AMNH FARB 30806 was not subjected to any chemical preparation procedures (including glues and consolidants) post collection to prevent chemical contamination. A small piece of the distal tip of a left primary wing feather was removed for scanning electron microscopy (Figure 1b). To minimise damage to the fossil, this area was chosen because of a natural break in the slab. The sample was not destroyed and remains with the main slab.

3.2. Synchrotron X-ray Fluorescence and X-ray Absorption Spectroscopy

Synchrotron analyses were undertaken at Stanford Synchrotron Radiation Lightsource (SSRL) beam line 6-2 and at Diamond Light Source (DLS) beam line I18. Our experimental setup and methods for the analysis of samples at these two facilities has been discussed extensively in previous studies⁵⁻¹². Additionally, Bergmann et al.¹² provides a comprehensive review of the techniques applied in this study. Analysis of AMNH FARB 30806 replicated the methods in these studies; a summary of those methods is discussed below.

Synchrotron Rapid Scanning X-ray Fluorescence (SRS-XRF) at SSRL wiggler beam line 6-2 has been optimized to perform 2D elemental imaging on the scale of decimeters at a resolution of 100 microns or less with an acquisition rate of about 30 s/cm². This allows entire surfaces of specimens (fossil or otherwise up to 60×60 cm) to be elementally mapped. SRS-XRF is particularly useful for fossils as they can be analysed in-situ with their embedding geological matrix without necessitating destructive sampling. This technique allows for elemental distributions affiliated with biological or geological processes to be visualized. A single element Vortex silicon drift detector was employed, which can detect the X-ray emissions of up to 16 elements simultaneously allowing those elements to be spatially mapped. For this experiment the elements that were mapped across the fossil and matrix included: silicon, phosphorus, sulfur, chlorine, potassium, calcium, titanium, manganese, iron, nickel, copper, zinc, arsenic, bromine, barium and mercury. The incident beam energy for the XRF imaging experiments was 13.5 keV optimized for detecting the K-edge emission of elements of atomic number 20 (Ca) to 80 (Hg)

1 and performed under ambient conditions (high Z). Lower atomic number elements (low Z) from
2 14 (Si) to 17 (Cl) were scanned at a beam energy of 3.15 keV with specimens enclosed within a
3 helium atmosphere to reduce attenuation of the incident beam and fluoresced signal. A beam
4 diameter of 100 μm was achieved using a tantalum pinhole. Spatial correlations from the
5 elemental maps were processed using ImageJ¹³ utilizing the Image CorrelationJ¹⁴ plugin.

6 Quantification and X-ray Absorption Near Edge Structure (XANES)¹⁵ spectroscopy of S
7 and Cu were also conducted at SSRL. Quantification was conducted under the same
8 experimental conditions as the elemental maps with a full Energy Dispersive Spectrometry
9 (EDS) spectrum collected for 100 live seconds for each location. Points were taken in both high
10 Z and low Z geometries on a number of matrix and fossil tissue types for quantitative analysis of
11 AMNH FARB 30806 (Figure 1a). The point analyses were fitted using PyMCA freeware¹⁶ and
12 calibrated against a mineral (Durango apatite) reference standard.

13 XANES spectroscopy at the S K α edge and the Cu K α edge were conducted to determine
14 oxidation states. Sulfur (K₂SO₄) and copper (Cu foil) standards were used to calibrate the energy
15 of the monochromator position. The sulfate peak position (2481.75 eV) was based on the K₂SO₄
16 standard. Organic sulfonate (2480.25 eV), sulfoxide (2474.35 eV) and thiol (2473.25 eV) were
17 calibrated on the K₂SO₄ standard and from published data^{5, 8, 17, 18}

18 Extended X-ray Absorption Fine Structure (EXAFS)¹⁵ spectroscopy at the Mn K α edge
19 was conducted at the Diamond Light Source (DLS) beamline I-18 using Kirkpatrick-Baez
20 mirrors to produce a beam spot size of 5 microns. EXAFS spectroscopy was conducted in order
21 to ascertain the coordination chemistry of Mn.

22 23 **3.3. Environmental Scanning Electron Microscopy (ESEM) with Energy Dispersive 24 Spectroscopy (ESEM-EDS)**

25 ESEM images and EDS quantification were acquired using a JEOL JSM-6400 with
26 Energy dispersive X-Ray (EDX) spectroscopy (Princeton Gamma Tech system). The sample was
27 uncoated and imaged in partial vacuum using backscatter or secondary electron detectors at an
28 accelerating voltage of either 12 or 15 keV. Semi-quantitative standard-less EDS analyses was
29 completed using an accelerating voltage of 15 keV for 100 live seconds.

30 31 **4. RESULTS**

1 Feather preservation in AMNH FARB 30806 is variable, with some feathers well
2 preserved (Figure 1c), while others have clearly decomposed (Figure 1a). Figure 1c shows one of
3 the well-preserved feathers with gradational preservation from well preserved with clear barbs to
4 more patchy organic areas in the general form of feathers. The fossil appears to exhibit
5 differences in lateral microfacies that resulted in a morphological preservation gradient or
6 'morpho-gradient'.

7 8 **4.1. Synchrotron X-ray Fluorescence and X-ray Absorption Spectroscopy**

9 SRS-XRF maps of AMNH FARB 30806 reveal that particular elements are constrained
10 within discrete biological structures while others follow a distribution consistent with geological
11 processes. Elements such as P, S, Ca, Cu and Zn occur within bones, feathers and the orbit (eye
12 socket) (Figure 2). The proximal portion of the rachi on the wings are clearly defined; however,
13 distally, feather preservation is poor (Figure 2). There are two well-preserved contour feathers
14 lying below the left wing where the rachi and barbs can be identified (Figure 1c, 2a). Cu is
15 distributed throughout the feathers with the most intensity proximally (Figure 2a). As expected
16 for bones (a hydroxyapatite), P is highly constrained to the bones and elevated relative to the
17 entombing matrix (Figure 2c). Ba, Ni, Mn, Cl and to a lesser extent, Br, are also associated
18 within the feathers of AMNH FARB 30806.

19 Quantification corroborates the maps and shows that P, S, Cl, Mn, Fe, Ni, Cu, Zn and Br
20 are elevated in the feather regions compared to the matrix (Table 1). Additionally, there are
21 elevated Mn, Ni, Cu, Zn, and Br within the orbit compared to the matrix. Lastly, P, S, Mn, Ni
22 and Zn in bone show higher levels than in the matrix.

23 24 **4.2. X-ray Absorption Near Edge Structure (XANES)**

25 Sulfur XANES (Figure 3) demonstrate the presence of 4 oxidation states for S: sulfate,
26 sulfonate, sulfoxide and thiol. The more reduced forms of S (sulfonate, sulfoxide and thiol)
27 appear only in preserved feathers and are not present in the matrix. Note that the peak above the
28 sulfate energy for one of the matrix spectra (Figure 3b) is most likely due a resonance feature at
29 the Pb M₅ edge (Pb concentrations range between 65 and 83 ppm; see Table 1). This is likely a
30 result of small amounts of Pb substituting for Ca in gypsum or anhydrite in the sedimentary
31 matrix. When the S XANES spectra are normalized to raw intensity (I / I_0) based on the sulfate

1
2
3 1 standard (Figure 3f), the relative intensities of the different sulfur species in the matrix are
4 appreciably lower than in any of the fossil feathers (Figure 3). The relatively low organic peak in
5 the matrix (Figure 3b) could be the result of either hitting a small fragmentary fossil just below
6 the surface of the matrix or of the breakdown and mass-transfer of organic S laterally from the
7 fossil tissues. However, only sulfoxide is present so this might suggest a different source for this
8 signal.

9
10
11
12
13
14 7 Copper XANES (Figure 4) suggest that Cu is present as an organometallic chelate bound
15 to organic O and/or N terminated functional groups in a similar manner to that seen in Wogelius
16 et al.⁸ and Manning et al.¹⁰, rather than as an inorganic compound such as Cu oxide. The Cu
17 XANES spectra for AMNH FARB 30806 are similar to the eumelanin standard and previously
18 published spectra from other Green River feathers (Figure 4)⁸. Both the Cu oxide and Cu foil
19 produce additional peaks that are characteristic of inorganically bound Cu and are not seen in the
20 Cu spectra for AMNH FARB 30806.

21
22
23
24
25
26
27 14 In contrast, Mn K-edge EXAFS taken from a feathered region (Figure 1b) indicates that
28 Mn is contained within an oxide precipitate. The local coordination environment of Mn is
29 comparable to that for Mn contained in birnessite, a common mineral where Mn(IV) is in six-
30 fold coordination with oxygen atoms at a distance of 1.874 angstroms. The strong second shell
31 backscatter exhibited in the Fourier transform of EXAFS shown on Figure 5 is completely
32 different from the weak low amplitude feature that would be expected for a transition metal
33 incorporated into an organometallic chelate. In this case the second shell is best fit by 6 Mn
34 atoms at 2.869 atoms distance, consistent with birnessite or a slightly disordered birnessite group
35 mineral. Taking account of a known birnessite three-legged multiple scattering path including O
36 and Mn of ~3.3 angstroms length significantly improved the fit. The Mn mapped on the fossil
37 feather is inorganic, and most likely results from post-mortem geochemical precipitation (Figure
38 5).

29 30 31 32 33 34 35 36 37 38 39 40 41 42 43 44 45 46 47 48 49 50 51 52 53 54 55 56 57 58 59 60

4.3. Environmental Scanning Electron Microscopy (ESEM) with Energy Dispersive Spectroscopy (ESEM-EDS)

Both microscopy of the feathers and ESEM-EDS reveal a predominantly carbonaceous film with diagenetic crystalline mineral precipitates found throughout the feathers (Figure 6). Elongate ovoids approximately 2 μm were also observed in a few discrete areas on the feathers

1 (Figure 6b, c). These structures are found on both the surface and within voids of the
2 sedimentary rock. The ESEM-EDS spectra reveal more abundant C, S, Mg and Ti in the feather
3 than within the matrix. In contrast, the matrix spectrum shows more abundant Ca, as expected in
4 limestone in a carbonate rich rock.

5. DISCUSSION

7 Synchrotron analyses show that there is a combination of endogenous and exogenous
8 chemistry comprising AMNH FARB 30806. S, P, Cu and Zn can be mapped within discrete
9 biological structures, i.e., feathers and bone, indicating that these elements are most likely
10 derived from the original biology of the organism (Figure 2). Sulfur XANES shows that the S
11 within the feathers is abundant and predominantly present as organically-bound, reduced forms
12 that are either absent from or present in only minute quantities within the matrix (Figure 3).

13 Copper is present as an organometallic chelate similar to that found other studies where it
14 has been interpreted as derived from eumelanin pigmentation and not as an inorganic species.
15 Previous studies have found organic Cu occurring in different locations within a single feather¹⁰
16 or within an entire bird⁸. Eumelanin dark pigmentation in animals and has been shown to chelate
17 divalent trace metals such as Cu^{8, 19, 20}. Concentrations of Cu in AMNH30806 feathers range
18 from 36-394 ppm, while the matrix only contains 6 ppm (Table 1). The abundance and
19 variability of Cu within the feathers suggests that the distribution of organic Cu relates to dark
20 pigmentation of the feathers during life. However, due to the variable preservation of the
21 feathers, especially in the wings, it is difficult to differentiate any patterning resulting from the
22 relative intensities of Cu (Figure 2a).

23 In combination with the SRS-XRF imaging, both the Cu and S XAS strongly indicate
24 that these elements are derived from the original organism and have not been introduced from
25 the surrounding environment during burial and subsequent fossilization. Correlation of Cu to
26 total S shows an R^2 value of 0.57, a reasonably strong correlation after ~50 million years of
27 burial. This high value is most likely due to S occurring in both the matrix and feathers as
28 inorganic and organic species, respectively, whilst the Cu is contained only within the organic-
29 rich areas of the feathers (Figures 2-3). The correlation of organic S species to Cu is likely to be
30 higher, as seen in previous studies⁵, a function of chelated trace-metal from pigments inhibiting
31 the breakdown of organic S rich keratin in the feather¹⁰. However, due to the large size of this

1 specimen we were unable to map the entire fossil again below the sulfate critical energy to test
2 this.

3 Phosphorus is constrained to the bones (Figure 2c), as would be expected for
4 hydroxyapatite, but is present in slightly quantities lower (~10 wt%) than expected for extant
5 birds (~11-20 wt%)²¹. Comparatively, P concentration within the matrix is less than 0.1 wt%
6 (Table 1). Previous studies have shown that P loss from bones occurs within different
7 geochemical environments^{7, 21} and this is likely the case in AMNH FARB 30806.

8 The feather preservation in AMNH FARB 30806 is variable, with some feathers well
9 preserved, while others have clearly undergone more decomposition (Figure 1). Figure 1c shows
10 one of the well-preserved feathers with gradational preservation from clear barbs to more patchy
11 organic areas in the general form of feathers. This demonstrates differences in lateral
12 preservation at the microfacies scale. This difference, although altering the morphological
13 appearance of the feathers, does not appear to have a large impact on the preservation of mapped
14 trace metals in the feathers (Figure 2), supporting their relative immobility in preserved tissues
15 (intact or degraded).

16 In addition to feathers, Cu and Zn are also concentrated within the orbit (eye) (Figure 2a-
17 b). The concentrations of these elements are elevated compared to the matrix but are within
18 range of the feathers (Table 1). The elevated levels may either be due to underlying feathers or
19 the original eye pigmentation. Avian eyes concentrate pigments in the vascular tunic (which
20 includes the iris, choroid and ciliary body) the pecten oculi and the retinal pigment epithelium²².
21 Many avian and non-avian dinosaur fossils from the Jehol Biota of North Eastern China display
22 large amounts of preserved pigment inside the orbits²³. It has been suggested that one of the
23 functions of melanosomes within pigmented portions of the eye include acting as a barrier
24 against sustained exposure to both visible and ultraviolet light as well as protection against
25 oxygen radicals^{22, 24, 25}. Elevated levels of Zn, in particular, have been shown to be an important
26 antioxidant and to help moderate light levels among other physiological functions²⁶.
27 Melanosomes have been previously reported in the eyes of a fossil bird²⁷, mosasaur²⁸ and fish^{8,}
28 ²⁹.

29 Manganese is among several metallic elements that are known porphyrin chelates in
30 melanin^{19, 20} but is also extremely common in geochemical systems. Initially, the distribution of
31 Mn in AMNH FARB 30806 appears to follow biological structures in a similar manner to Cu

1 and S (Figure 7). This could be interpreted as Mn being derived from melanin. However, the Mn
2 EXAFS presented here show Mn is present as an inorganic oxide (Figure 5). Thus, the presence
3 of Mn in fossils may not necessarily indicate geochemical precipitation post-burial. Reduced
4 fluids most likely flowed through the slightly more permeable bed containing the fossil and
5 became oxidized in the void space due to the presence of slightly elevated oxygen levels. This
6 would oxidize soluble Mn(II) to insoluble Mn(IV) and cause the Mn-oxides to nucleate on the
7 fossil material. This result shows the importance of XAS analysis in partnering with the imaging
8 data so as to differentiate inorganic precipitates from biologically derived material.

9 ImageJ correlation analyses between selected elements also strongly indicates
10 precipitation of inorganic compounds post burial. Ba is indicative of inorganic precipitates and
11 its correlation with Mn ($R^2 = 0.80$) and Ni ($R^2 = 0.68$) supports that these other two elements
12 may also be inorganically derived and may be part of the same phase of elemental influx. In
13 previous studies Ni has been proposed to be endogenous in fossil birds based on correlation with
14 Cu and organic S¹⁰. However, this does not suggest that elevated Ni concentration in all cases is
15 exclusively either organically or inorganically derived. Rather, different taphonomic processes
16 may result in variable preservation, alteration, removal and precipitation of certain trace metals.
17 The relative location of Ba, Ni and Mn along the bones and feather rachis suggests that these
18 biological structures allowed for a preferential diagenetic fluid path. This, in turn, allowed for the
19 precipitation of these elements in addition to others such as Br and Cl. A number of cases of
20 geochemical precipitation within fossil specimens have been discussed previously (e.g.
21 Bergmann et al.⁷), this particular specimen however provided a unique test of our methodology
22 because the Mn precipitates so closely mimicked the biological structures.

23 Many previous studies on fossil pigments have focused on the melanin pigment
24 containing organelles, melanosomes (e.g. Vinther et al.²⁷, Clarke et al.³⁰, Li et al.³¹, Zhang et
25 al.³², Barden et al.³³, Carney et al.³⁴, Glass et al.³⁵, McNamara³⁶). The majority of the feathers
26 examined show a desiccated carbonaceous film with diagenetic mineral crystals (Figure 6). In
27 AMNH FARB 30806 there is little evidence of possible eumelanosomes (elongate organelles
28 associated with dark pigmentation) and no phaeomelanosomes (circular organelles associated
29 with light pigmentation) (Figure 6b-c). The putative eumelanosomes appear as external moulds
30 of the elliptical organelles; however, due to the advanced degradation of the feathers in AMNH
31 FARB 30806, it is difficult to ascertain whether these structures occur within the feather or

1 within the sediment. Identifying the location of these structures is important, as one of the only
2 ways to differentiate between melanosomes and morphologically similar bacteria, is the location
3 (i.e., inside the keratinous sheath or outside, respectively) of the structures³⁷. ESEM-EDS results
4 show S being present within the moulds; however EDS cannot determine S oxidation state and
5 so this S could either have an organic or inorganic affinity. The Cu SRS-XRF maps show that
6 there is Cu present in the feathers analyzed under ESEM (Figure 2a, upper box) but the
7 resolution was not enough to identify any organelles. Therefore, it is inconclusive whether the
8 ellipsoidal structures are external moulds of eumelanosomes or some other organic product. The
9 presence of C and S that maps within discrete biological structures might either be a function of
10 endogenous tissue preservation or possible bacterially mediated exogenous overprint, albeit both
11 due to biological processes.

12 13 6. CONCLUSION

14 The preservation of soft tissues in fossils is a function of the interplay between
15 biochemical and geochemical processes within a complicated series of events that begin at the
16 moment of death. AMNH FARB 30806, although well preserved, may not necessarily be
17 considered to be exceptional, but nonetheless provides important information on the taphonomy
18 of birds in the Green River Formation. Upon visual inspection, the feathers appear to be poorly
19 preserved with some rachi and barbs definable and only two distinct individual feathers.
20 However, elemental maps show that some endogenous elements reduce the ambiguity of
21 biological structures, such as P in the bone and S and Cu in the feathers. The local coordination
22 chemistry of S and Cu show that they are organically bound, most likely from the remnants of
23 keratin and eumelanin, respectively. Unlike other specimens¹⁰ where geochemically sourced
24 elements do not correlate with biological structures, the geochemical association in AMNH
25 FARB 30806 is much stronger. This study has been able to clearly differentiate between organic
26 remains from those overprinted by geochemical precipitates. In particular, Mn has been revealed
27 as an Mn oxide, birnessite or closely related mineral, rather than an organometallic chelate even
28 though it appears to be distributed within biological structures. Additional exogenous elements
29 include Ba, Br and Ni that map along the bones and feathers, with the organic remains acting as
30 nucleation sites for the geochemical precipitates. Finally, careful analysis must be conducted in

1
2
3 1 order to accurately unpick the taphonomic history of fossils, using the quantification and
4 2 distribution of chemistry to provide insight to the biology and biochemistry of ancient life.
5
6
7 3

4 7. ACKNOWLEDGMENTS

5 We would like to thank Carl Mehling from the American Museum of Natural History for his help
6 in the preservation of this fossil. We would also like to thank Dr. Karen Rosenthal for her helpful
7 discussions on avian anatomy and physiology. Additionally, we would like to thank NERC
8 (grant number NE/J023426/1), STFC, Diamond Lightsource and SLAC National Accelerator
9 Laboratory for their support. Portions of this work have been carried out at the Stanford
10 Synchrotron Radiation Lightsource, a National User Facility operated by Stanford University on
11 behalf of the U.S. Department of Energy, Office of Basic Energy Sciences.
12
13
14

14 8. REFERENCES

- 15
16 1. A. K. Behrensmeyer, S. M. Kidwell, R. A. Gastaldo, D. H. Erwin and S. L. Wing, *Paleobiology*,
17 2000, 26, 103-147.
18 2. A. K. Behrensmeyer, in *Taphonomy: Releasing the Data Locked in the Fossil Record*, eds. P. A.
19 Allison and E. G. Briggs, Plenum Press, New York, 1991, vol. 9, ch. 6, pp. 291-335.
20 3. P. L. Manning, P. M. Morris, A. McMahon, E. Jones, A. Gize, J. H. S. Macquaker, G. Wolff, A.
21 Thompson, J. Marshall, K. G. Taylor, T. Lyson, S. Gaskell, O. Reamtong, W. I. Sellers, B. E. van
22 Dongen, M. Buckley and R. A. Wogelius, *Proceedings of the Royal Society B: Biological*
23 *Sciences*, 2009, DOI: 10.1098/rspb.2009.0812.
24 4. L. Grande, *The Lost World of Fossil Lake: Snapshots from the Past*, The University of Chicago
25 Press, 2013.
26 5. N. P. Edwards, P. Manning, U. Bergmann, P. Larson, B. E. van Dongen, W. I. Sellers, S. M.
27 Webb, D. Sokaras, R. Alonso-Mori, K. Ignatyev, H. E. Barden, A. van Veelen, J. Anné, V. M.
28 Egerton and R. A. Wogelius, *Metallomics*, 2014, 6, 774-782.
29 6. N. P. Edwards, R. A. Wogelius, U. Bergmann, P. Larson, W. I. Sellers and P. L. Manning, *Appl.*
30 *Phys. A*, 2013, 111, 147-155.
31 7. U. Bergmann, R. W. Morton, P. L. Manning, W. I. Sellers, S. Farrar, K. G. Huntley, R. A.
32 Wogelius and P. Larson, *Proceedings of the National Academy of Sciences*, 2010, 107, 9060-
33 9065.
34
35
36
37
38
39
40
41
42
43
44
45
46
47
48
49
50
51
52
53
54
55
56
57
58
59
60

- 1
2
3 1 8. R. A. Wogelius, P. L. Manning, H. E. Barden, N. P. Edwards, S. M. Webb, W. I. Sellers, K. G.
4 2 Taylor, P. L. Larson, P. Dodson, H. You, L. Da-qing and U. Bergmann, *Science*, 2011, 333,
5 3 1622-1626.
6
7
8 4 9. N. P. Edwards, H. E. Barden, B. E. van Dongen, P. L. Manning, P. L. Larson, U. Bergmann, W. I.
9 5 Sellers and R. A. Wogelius, *Proceedings of the Royal Society B: Biological Sciences*, 2011, 278,
10 6 3209-3218.
11
12 7 10. P. Manning, N. P. Edwards, R. A. Wogelius, U. Bergmann, H. E. Barden, P. Larson, D. Schwarz-
13 8 Wings, V. M. Egerton, D. Sokaras, R. A. Mori and W. I. Sellers, *Journal of Analytical Atomic*
14 9 *Spectrometry*, 2013, 28, 1024-1030.
15
16 10 11. J. Anné, N. P. Edwards, R. A. Wogelius, A. R. Tumarkin-Deratzian, W. I. Sellers, A. van Veelen,
17 11 U. Bergmann, D. Sokaras, R. Alonso-Mori, K. Ignatyev, V. M. Egerton and P. L. Manning,
18 12 *Journal of The Royal Society Interface*, 2014, 11.
19
20 13 12. U. Bergmann, P. L. Manning and R. A. Wogelius, *Annual Review of Analytical Chemistry*, 2012,
21 14 5, 361-389.
22
23 15 13. C. A. Schneider, W. S. Rasband and K. W. Eliceiri, *Nat Meth*, 2012, 9, 671-675.
24
25 16 14. G. Chinga and K. Syverud, *Nordic Pulp and Paper Research Journal*, 2007, 22, 441-446.
26
27 17 15. J. J. Rehr and R. C. Albers, *Reviews of Modern Physics*, 2000, 72, 621-654.
28
29 18 16. V. A. Solé, E. Papillon, M. Cotte, P. Walter and J. Susini, *Spectrochimica Acta Part B: Atomic*
30 19 *Spectroscopy*, 2007, 62, 63-68.
31
32 20 17. M. Sandström, F. Jalilehvand, E. Damian, Y. Fors, U. Gelius, M. Jones and M. Salomé,
33 21 *Proceedings of the National Academy of Sciences of the United States of America*, 2005, 102,
34 22 14165-14170.
35
36 23 18. K. M. Wetherall, R. M. Moss, A. M. Jones, A. D. Smith, T. Skinner, D. M. Pickup, S. W.
37 24 Goatham, A. V. Chadwick and R. J. Newport, *Journal of Archaeological Science*, 2008, 35,
38 25 1317-1328.
39
40 26 19. G. E. Hill and K. J. McGraw, *Bird Coloration: Mechanisms and measurements*, Harvard
41 27 University Press, 2006.
42
43 28 20. M. Niecke, M. Heid and A. Krüger, *J Ornithol*, 1999, 140, 355-362.
44
45 29 21. M. B. Goodwin, P. G. Grant, G. Bench and P. A. Holroyd, *Palaeogeography, Palaeoclimatology,*
46 30 *Palaeoecology*, 2007, 253, 458-476.
47
48 31 22. M. P. Jones, K. E. Pierce Jr and D. Ward, *Journal of Exotic Pet Medicine*, 2007, 16, 69-87.
49
50 32 23. P.-j. Chen, Y. Wang, Y.-q. Wang and M.-M. Chang, eds., *The Jehol Fossils: The Emergence of*
51 33 *Feathered Dinosaurs, Beaked Birds and Flowering Plants*, Academic Press, London, 2008.
52
53 34 24. S. G. Kiama, J. Bhattacharjee and K. D. Weyrauch, *Journal of Anatomy*, 1994, 185, 637-642.
54
55 35 25. D.-N. Hu, J. D. Simon and T. Sarna, *Photochemistry and Photobiology*, 2008, 84, 639-644.
56
57
58
59
60

- 1
2
3 1 26. B. H. Grahn, P. G. Paterson, K. T. Gottschall-Pass and Z. Zhang, *Journal of the American*
4 2 *College of Nutrition*, 2001, 20, 106-118.
5
6 3 27. J. Vinther, D. E. G. Briggs, R. O. Prum and V. Saranathan, *Biology Letters*, 2008, 4, 522-525.
7
8 4 28. J. Lindgren, M. W. Caldwell, T. Konishi and L. M. Chiappe, *PLoS ONE*, 2010, 5, e11998.
9
10 5 29. J. Lindgren, P. Uvdal, P. Sjövall, D. E. Nilsson, A. Engdahl, B. P. Schultz and V. Thiel, *Nat*
11 6 *Commun*, 2012, 3, 824.
12
13 7 30. J. A. Clarke, D. T. Ksepka, R. Salas-Gismondi, A. J. Altamirano, M. D. Shawkey, L. D'Alba, J.
14 8 Vinther, T. J. DeVries and P. Baby, *Science*, 2010, 330, 954-957.
15
16 9 31. Q. Li, K.-Q. Gao, J. Vinther, M. D. Shawkey, J. A. Clarke, L. D'Alba, Q. Meng, D. E. G. Briggs
17 10 and R. O. Prum, *Science*, 2010, 327, 1369-1372.
18
19 11 32. F. Zhang, S. L. Kearns, P. J. Orr, M. J. Benton, Z. Zhou, D. Johnson, X. Xu and X. Wang,
20 12 *Nature*, 2010, 463, 1075-1078.
21
22 13 33. H. E. Barden, R. A. Wogelius, D. Li, P. L. Manning, N. P. Edwards and B. E. van Dongen, *PLoS*
23 14 *ONE*, 2011, 6, e25494.
24
25 15 34. R. M. Carney, J. Vinther, M. D. Shawkey, L. D'Alba and J. Ackermann, *Nat Commun*, 2012, 3,
26 16 637.
27
28 17 35. K. Glass, S. Ito, P. R. Wilby, T. Sota, A. Nakamura, C. Russell Bowers, K. E. Miller, S. Dutta, R.
29 18 E. Summons, D. E. G. Briggs, K. Wakamatsu and J. D. Simon, *Organic Geochemistry*, 2013, 64,
30 19 29-37.
31
32 20 36. M. E. McNamara, *Palaeontology*, 2013, 56, 557-575.
33
34 21 37. A. E. Moyer, W. Zheng, E. A. Johnson, M. C. Lamanna, D.-q. Li, K. J. Lacovara and M. H.
35 22 Schweitzer, *Sci. Rep.*, 2014, 4.
36
37
38
39
40
41
42
43
44
45
46
47
48
49
50
51
52
53
54
55
56
57
58
59
60

9. TABLE AND FIGURES

Table 1: XRF Point Analyses. The numbers beside the feature correspond to the points marked on Figure 1a. Beamline geometry is calibrated using a Durango apatite standard. 2σ errors, calculated from counting statistics, are approximately 8% relative for the light elements (Ca, Si, P, S, Cl) and 5% for all of the trace metals except Pb. (For example, the Ca wt. % in the bone is $37.9 \pm 3\%$ while the Zn concentration is 51 ± 2.6 ppm.) Errors on Pb, due to overlap with As and

1
2
3 1 rising background caused by the elastic and Compton scattering peaks, are much larger at
4
5 2 approximately 25% (using the bone example: 64 ± 16 ppm).
6
7
8 3
9
10 4

11 Figure 1: AMNH FARB 30806. (A) Coliiformes bird (AMNH FARB 30806) from the Green
12 River Formation, Fossil Butte Member. The numbers correspond to where point data was taken
13 for High Z (1-7) and Low Z (8-12) elements. Scale bar = 5 cm. (B) Magnified view of the upper
14 box containing the feather sample obtained for SEM. (C) Magnified view of well preserved
15 feathers. (B-C) Scale bar = 2 cm.
16
17
18
19
20
21
22

23 11 Figure 2: SRS-XRF Elemental maps of AMNH FARB 30806. (A) Copper (red) and (B) zinc
24 12 (green) maps showing the relative intensities of the elements mapping distinctly within the
25 13 feathers. (A) The upper box in copper corresponds to Figure 1b, while the lower box corresponds
26 14 to Figure 1c. The lower arrow is pointing to the rachis of a feather. (C) Phosphorus (blue) and
27 15 sulfur (yellow) elemental map distinctly showing bone with higher intensities of phosphorus and
28 16 the feathers containing higher intensities of sulfur. (A-C) Upper arrow is pointing to the orbit
29 17 (eye socket). Scale bar = 5 cm.
30
31
32
33
34
35
36

37 19 Figure 3: Sulfur XANES for AMNH FARB 30806. The relative abundance of sulfur within the
38 20 matrix (a-b) and feathers (c-e) has been calibrated to a sulfur standard, K_2SO_4 (f). The data are
39 21 normalized to raw intensity I/I_0 . The two matrix samples both have peaks that correspond with
40 22 the sulfate standard, while the feathers contain abundant sulfonate, sulfoxide and thiol relative to
41 23 the matrix samples. The lower matrix spectrum (a) shows an elongate organic peak across both
42 24 sulfoxide and thiol due to the breakdown of organics. The upper matrix spectrum (b) has an
43 25 additional peak at 2485 eV, which is due to Pb substitution for Ca in $CaSO_4$.
44
45
46
47
48
49
50

51 27 Figure 4: Copper XANES spectra. Cu XANES spectra are from a copper standard (copper foil)
52 28 and three different feathers from AMNH FARB 30806. The spectra from these have been plotted
53 29 along with published spectra from copper oxide, natural copper eumelanin, and two isolated
54
55
56
57
58
59
60

1
2
3
4 1 feathers from the Green River Formation (BHI 6358 and 6403)⁸. The arrows on the copper oxide
5 2 are pointing to peaks that are unique to that spectrum and do not occur in the fossil material.
6
7 3

8
9 4 Figure 5: Mn EXAFS. Three panel results of EXAFS analysis of Mn within the fossil specimen.
10 5 (A) Raw data for the absorption coefficient measurement at the Mn K-edge. (B) EXAFS function
11 6 presented for the specimen (solid line) and a computed fit to the data (dashed line). (C) Fourier
12 7 transform of EXAFS where the data are presented as the discrete points and the best fit is shown
13 8 as the thin solid line. Clearly the RDF shows two strong backscattering shell surrounding the
14 9 central Mn absorber.
15
16
17
18
19 10

20
21 11 Figure 6: SEM of feathers from AMNH FARB 30806. (A) Secondary electron image of a
22 12 carbonaceous film, mineral crystals and possible eumelanosomes (arrow). Scale bar = 50 μm . (B)
23 13 Backscattered electron image of possible eumelanosome preservation (arrow). Scale bar = 10
24 14 μm . (C) Secondary electron image of possible eumelanosome preservation (arrow). Scale bar = 5
25 15 μm .
26
27
28
29
30 16

31
32 17 Figure 7: Copper and manganese elemental map of AMNH FARB 30806. Copper (red) and
33 18 manganese (white) both appear to map within the feathers; however correlation between the two
34 19 show no significance in the distribution. Scale bar = 5 cm.
35
36
37
38
39
40
41
42
43
44
45
46
47
48
49
50
51
52
53
54
55
56
57
58
59
60